High temperature tribological properties of silicon nitride in dry sliding contact against Inconel 718 heated by laser

Bin Zhao[a], Iyas Khader[b,a], Rahul Raga[a], Georg Konrath[a], Ulrich Degenhardt[c], Andreas Kailer[a]

[a] Fraunhofer Institute for Mechanics of Materials IWM, Wöhlerstraße 11, 79108 Freiburg, Germany

[b] Department of Industrial Engineering, German-Jordanian University, P. O. Box35247, 11180 Amman, Jordan

[c] FCT Ingenieurkeramik GmbH, Gewerbepark 11, 96528 Frankenblick, Germany

Abstract

Ceramic tools have been successfully applied in laser-assisted machining of nickel-based alloys. However, few studies have addressed high temperature dry frictional behavior of ceramics against nickel-based alloys. In this study, tribological tests of silicon nitride in dry sliding against both laser-heated (600 °C) and unheated Inconel 718 were carried out. The tribological properties at sliding velocities ranging from 2.5 m/s to 10 m/s were investigated. A finite element simulation model of sliding contact was considered to obtain localized contact surface temperatures. The combination of experimental and numerical results enabled evaluating and analyzing the wear behavior.

The results showed that the laser heating modifies the temperature distribution resulting in reduced wear rates of the ceramic up to a critical sliding velocity (7.5 m/s in this particular case). With increasing sliding velocity, a tribochemical layer forms, and becomes thick and unstable, resulting in higher wear of the ceramic at a lower coefficient of friction.

Keywords: silicon nitride; Inconel 718; tribochemical wear; dry sliding; high temperature; laser heating

1 Introduction

Nickel-based superalloys are typically difficult-to-cut materials. Due to their exceptional high-temperature properties, ceramic tools have been widely applied in high-speed machining of nickel-based superalloys [1, 2]. Nevertheless, high cutting temperatures engendered during machining nickel-base superalloys at high speeds can still adversely affect the ceramic tool properties (e.g., hardness and fracture toughness) [3], thus, limiting the tool life [2]. Currently, alumina-based ceramics (e.g., Al_2O_3/SiC whisker) [4], silicon nitride ceramics and silicon nitride-based ceramic tools (e.g., SiAlON) [5] are used for machining applications. However, silicon nitride based ceramic tools outperform alumin-based ceramic tools due to their higher strength and toughness, lower coefficient of thermal expansion and better thermal shock resistance [6], hence, exhibit better notch wear resistance [7], but rather lower flank wear resistance due to low hardness and less chemical stability [8].

Many researchers have demonstrated that laser-assisted machining (LAM) can improve the machinability of difficult-to-cut materials such as nickel-based superalloys, which yields an improved surface roughness, decreased cutting energy, and increased tool life [9, 10]. Due to good high temperature properties and chemical stability, ceramic tools show better performance in comparison to carbide tools in LAM of nickel-based superalloys [11, 12]. Anderson et al. [10] found that notch wear and flank wear of ceramic tool in LAM of Inconel 718 can be reduced by increasing the material removal temperature up to 540 °C and the cutting velocity from 1 to 3 m/s. It is worth noting though that LAM does not always improve the ceramic tool life. The tool wear rate can be higher than that in conventional machining if the cutting speed is above a critical speed [13].

The ceramic tool wear in LAM of Inconel 718 is mainly affected by the high temperature frictional characteristics between the ceramic and the alloy. Huang et al. [14] investigated the tribological behavior of silicon nitride ceramic in dry sliding against various superalloys from ambient temperature to 800 °C. It was found that high contact temperature promoted the formation of a tribochemical layer on the tool surface which protects the ceramic surface and cause reduction in wear rates. Shabaly et al. [15] studied the wear of SiAlON ceramic tools in dry high-speed machining of a nickel-based alloy and also found that the formation of tribo-films on the tool surface provided a thermal barrier. Similar tribochemical layers were reported by Khader et al. [16] in silicon nitride and Renz et al. [17] in SiAlON in studying the tribological properties of ceramics sliding against Inconel 718. In both studies, it was concluded that an increase in sliding velocity gives rise to higher contact temperatures and causes the tribochemical layers to become unstable and result in high wear rates attributed to tribochemical wear. Çelik et al. [18] found that a diffusion layer was formed in high speed machining of Inconel 718 with SiAlON ceramic tools. The wear rates were accelerated due to the formation and removal of this diffusion layer.

It appears that a tribochemical layer caused by diffusion and oxidation at high temperatures has a great impact on the tribological properties of silicon nitride based ceramics. Currently, there are very few studies on the wear behavior of ceramics in dry sliding against nickel-based alloys at high temperatures [14]. The primary objective of this work is to study the tribological properties of silicon nitride based ceramics in dry sliding against laser-heated Inconel 718. Considering the possibility of formation of a tribochemical layer at high temperatures, a low glassy-phase silicon nitride material system was used in this work, aiming at addressing the frictional process of silicon nitride. To better explain the experimental findings, a numerical simulation model for the calculation of surface contact temperature was employed. This work can provide fundamental knowledge in using or developing silicon nitride based ceramic tools in specific machining operations such as laser-assisted machining of nickel-based alloys.

2 Experimental

2.1 Sliding contact experiments

A commercially available silicon nitride material (SN-PU, FCT Ingenieurkeramik GmbH Germany) was used in this work. SN-PU ceramic has a fine microstructure composed of β-Si_3N_4 phase and a low fraction of sintering aids (Al_2O_3 and Y_2O_3, ≤2.5 wt.%). The microstructure of SN-PU ceramic is shown in a backscattered mode scanning electron microscope (SEM) image in Fig. 1. The density is 3.21 g/cm^3, the typical crystal length is from 1 µm to 4 µm, and the average crystal aspect ratio is 3. The room-temperature hardness (HV 20) and fracture toughness (Nihara and Morena [19]) of SN-PU are 15.9 GPa and 6.0 MPa·m$^{1/2}$, respectively.

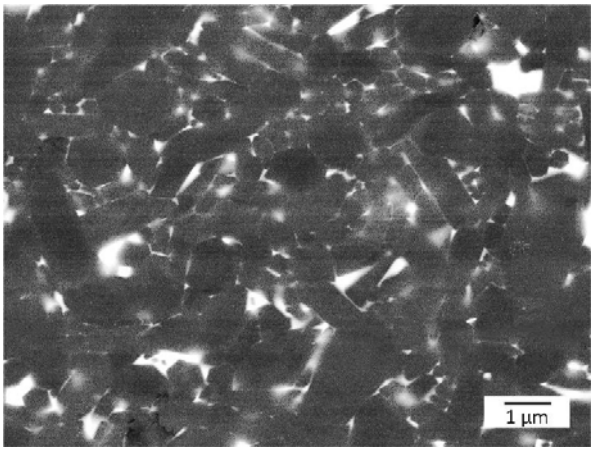

Fig. 1 Backscattered SEM image of the microstructure of SN-PU ceramic

Pin-on-disk (room and high temperature) experiments were carried out to study the tribological properties of silicon nitride in dry sliding against Inconel 718. The chemical composition of Inconel 718 is listed in Table 1.

Table 1 Chemical composition of Inconel 718

Element	C	Si	Mn	Ni	Co	Cr	Al	Ti	Mo	Nb	Cu	Fe and others
Content (wt.%)	0.036	0.19	0.05	51.17	<1.0	19.02	0.60	1.00	3.07	5.01	0.02	Balance

The ceramic pin with a CNGN-type insert geometry is shown in Fig. 2a. The test setup is schematically illustrated in Fig. 2b and shown in Fig. 2c. Two sets of experiments were conducted: with a laser-heated disk (HT-tests) and without heating (RT-tests). In the heated experiments, laser (Laserline, LDL 80-1000 diode laser) was used to heat the Inconel 718 disk on the radially opposite side of the contact zone. A pyrometer was used to measure the temperature of the disk prior to contact and provide feedback to the controller to maintain a desired temperature of 600 °C. In both sets of experiments, the ceramic

sample was not heated and it was fixed into the tribometer using a special fixture designed to withstand the tangential forces emerging from dry sliding.

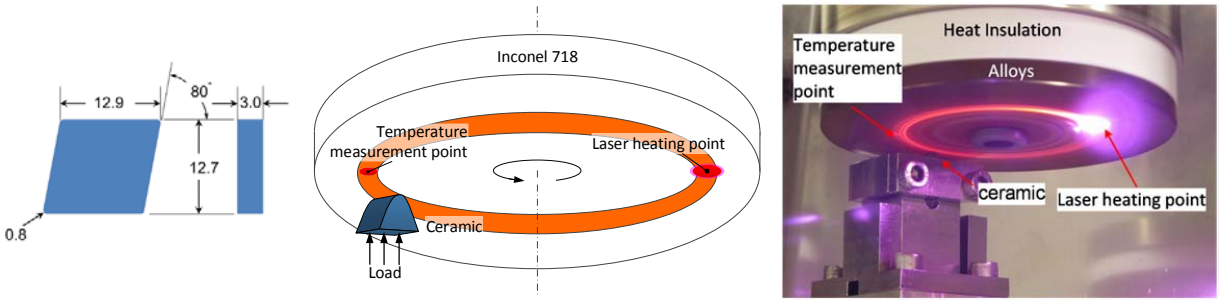

(a) (b) (c)

Fig. 2 (a) SN-PU ceramic sample geometry, (b) the pin-on-disk test configuration, and (c) sliding-contact experiment.

A 3 mm line contact is created between the edge of the ceramic pin and the flat surface of metallic disk. A normal force of 100 N was applied during the test, which is comparable with the loads exerted on ceramic tools in high-speed machining processes. The sliding speed was varied from 2.5 m/s to 10 m/s and the sliding distance was 2000 m for each experiment. A summary of the experimental parameters is given in Table 2. Each set of experiments was repeated three times. The width of specimen's wear land (width of the contact surface) was measured to calculate the wear volume on the ceramic sample. The friction coefficient was recorded by the tribometer. The friction coefficient was plotted after averaging test data.

Table 2 Experimental parameters of the sliding-contact experiments

Material pair	SN-PU/Inconel 718
Normal applied load (N)	100
Sliding velocity of the ceramic samples (m/s)	2.5, 5.0, 7.5, 10.0
Sliding distance (m)	2000
Temperature (°C)	600, 25 (room temperature)
Lubricant	Dry sliding
Atmosphere	Air

The worn ceramic samples were embedded and then polished to conduct cross-sectional analysis. Scanning electron microscopy (SEM) and energy-dispersive X-ray spectroscopy (EDX) were carried out to observe the microstructure and chemical constituents on the worn contact surfaces and cross sections of the ceramic samples.

2.2 Finite element simulations of sliding contact

The localized contact surface temperature is almost impossible to measure accurately; hence, finite element (FE) analysis represents a suitable method to obtain a rough estimate of contact temperatures. Sliding contact was modeled using a coupled thermal-mechanical two-dimensional plane-stress finite element simulation in ABAQUS/Standard. A normal force of 100 N along a contact line of 3 mm was applied on the ceramic tool; the sliding velocity was set to 5 m/s. In the simulation model, frictional heat generation with a weighting factor for distribution of the heat between the interacting surfaces of f=0.5 and a fraction of dissipated energy converted into heat η=0.5 were assumed. More details on the selection of these parameters can be found in [16].

For conduction between the ceramic and metal, an interface conductance was assumed to be pressure dependent with values in the range between h_{ic}=1500 W/m^2·K and h_{ic}=8500 W/m^2·K [20]. The convection heat transfer to the surrounding air was accounted for by calculating an approximate natural convection heat transfer coefficient ($\bar{h}_{nc}$=15 W/m^2·K) at a sink temperature of T_{SC}=20 °C. Radiation was incorporated into the thermal model by assuming a sink temperature of T_{SR}=293.15 K. Emissivity values of 0.9 and 0.5 were adopted for silicon nitride [21, 22] and Inconel 718 [23], respectively. Temperature-dependent elastic modulus and thermo-physical properties for SN-PU were measured in [24] and shown in Fig. 3; its thermal expansion coefficient was measured and found to be 1.9×10^{-6} K^{-1} and 3.0×10^{-6} K^{-1} at 200 °C and 1000 °C, respectively. Inconel 718 temperature-dependent properties were obtained from [25].

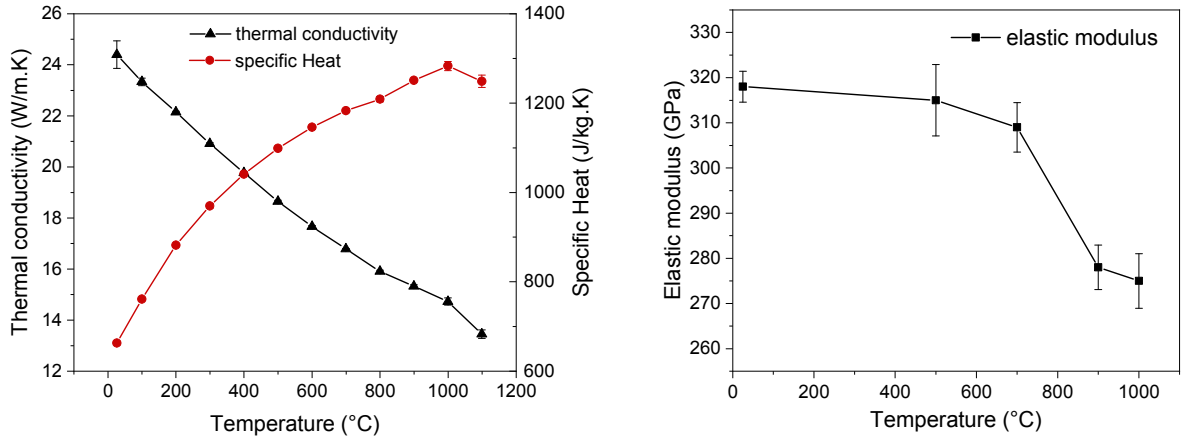

(a) (b)

Fig. 3 (a) Elastic modulus, and (b) thermophysical properties of SN-PU **[24]**

To simulate the HT-tests (Inconel 718 disk heated and maintained at 600 °C), Fig. 4 illustrates the boundary conditions of the sliding contact simulation. The initial temperatures of Inconel 718 and silicon nitride were set to 600 °C and 25 °C, respectively. The area included within the dotted lines in Fig. 4 was

maintained using boundary conditions at 600 °C to simulate laser heating. The temperature of the rest of the contact surfaces was released throughout the simulation to model heat transfer.

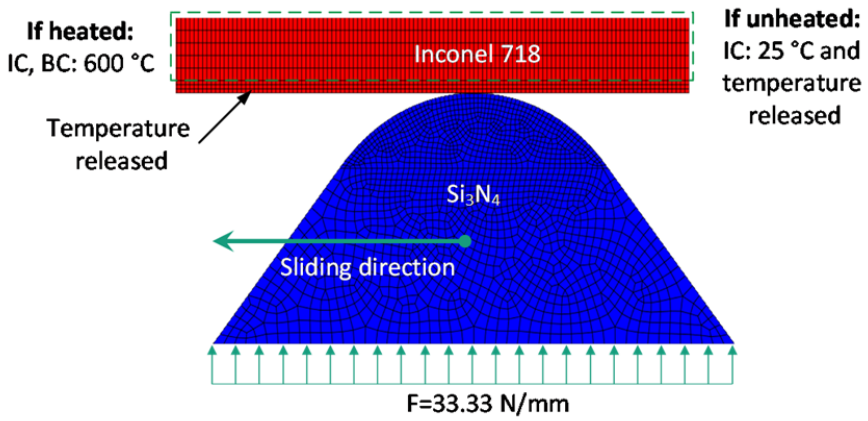

Fig. 4 FE mesh and contact configuration in the FE simulation.

For the RT-tests simulations, an initial temperature of 25 °C was assumed for both contact partners; temperature boundary conditions were released throughout the simulations.

Coulomb friction was assumed between the surfaces in contact with a constant COF obtained from the experiments. The COF was set to $\mu = 0.34$ and $\mu = 0.54$ for the HT-tests and RT-tests, respectively. A siding distance of 200 mm was simulated.

3 Results

3.1 Dry sliding experiments

The coefficient of friction (COF) for HT-tests as function of sliding distance for different sliding velocities is shown in Fig. 5a. The value and scatter of the COF decrease with increasing sliding velocity. The mean value of the COF plotted against the sliding velocity is shown in Fig. 5b. At same sliding velocity, the mean value and scatter of COF in HT-test is much smaller than that in RT-test. The smaller scatter in COF means that friction between the pin and disk is more stable at higher disk temperature.

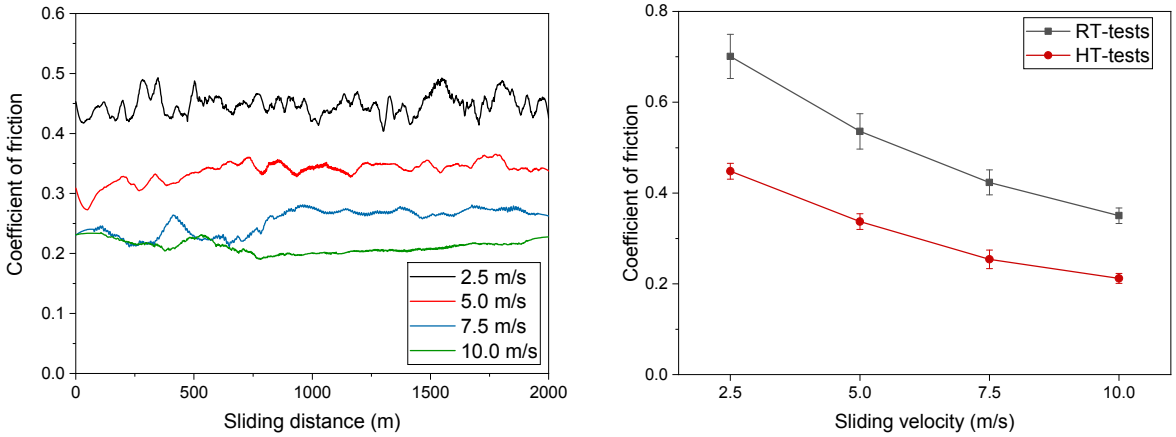

(a) (b)

Fig. 5 (a) COF plotted against sliding distance (HT-tests) and (b) mean value of COF for HT-tests and RT-tests.

The sliding velocity dependence of the wear volume of the ceramic is plotted in Fig. 6. The wear volume of SN-PU ceramic in RT-test decreases continuously with increasing sliding velocity. The wear volume of SN-PU ceramic in HT-test decreases and then increases. The sliding velocities corresponding to the lowest wear is 7.5 m/s. The wear volumes of SN-PU ceramic in HT-tests are smaller than those in RT-test up to 7.5 m/s, and the opposite is true at a velocity of 10.0 m/s. The wear difference between HT-test and RT-test becomes smaller with sliding velocity increasing to 7.5 m/s, which means the advantage of heating the metallic disk becomes gradually unremarkable.

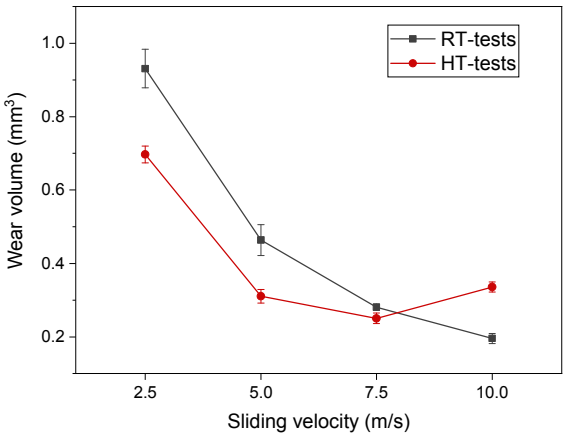

Fig. 6 Wear volume of the ceramic plotted against sliding velocity for HT-tests and RT-tests.

The surface coverage percentage of the adhered transfer layer (metallic tribolayer) on the ceramic surface plotted against sliding velocities is shown in Fig. 7. In both experiments, the area covered by the transfer layer decreases with increasing sliding velocities.

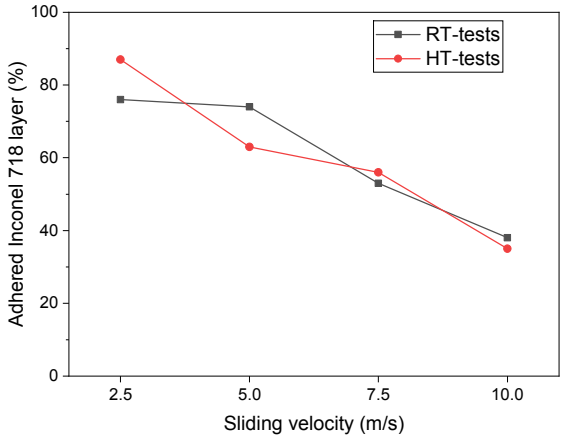

Fig. 7 Surface coverage percentage of adhered Inconel 718 layer (metallic transfer layer) on ceramic surface.

The frictional power ($P=\mu \cdot F_N \cdot v$) plotted against sliding velocities is shown in Fig. 8. As can be seen from the figure, the frictional power increases with increasing sliding velocity, and the frictional power in RT-tests is higher than that in HT-tests.

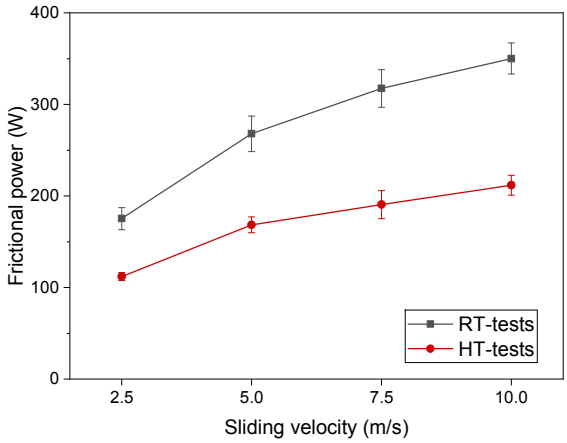

Fig. 8 Frictional power plotted against sliding velocity for HT-tests and RT-tests.

3.2 Numerical results

The contact surface temperature of the ceramic pin has reached steady-state after ca. 200 mm sliding distance. The results of the FE simulations obtained at a sliding velocity of 5 m/s are shown in Fig. 9. At a same sliding velocity, the temperature rise of both the ceramic and Inconel 718 in HT-tests is smaller than that computed for RT-tests. The maximum contact surface temperature of the ceramic in HT-tests reached 1470 °C, compared to ca. 2000 °C in RT-tests (Fig. 9a). However, due to the heating of Inconel 718 to 600 °C, its maximum contact surface temperature reached 645 °C (Fig. 9b) compared to 155 °C in RT-tests (Fig. 9c); hence, the temperature difference after sliding 200 mm was ca. 45 °C and 130 °C in HT-tests and RT-tests, respectively.

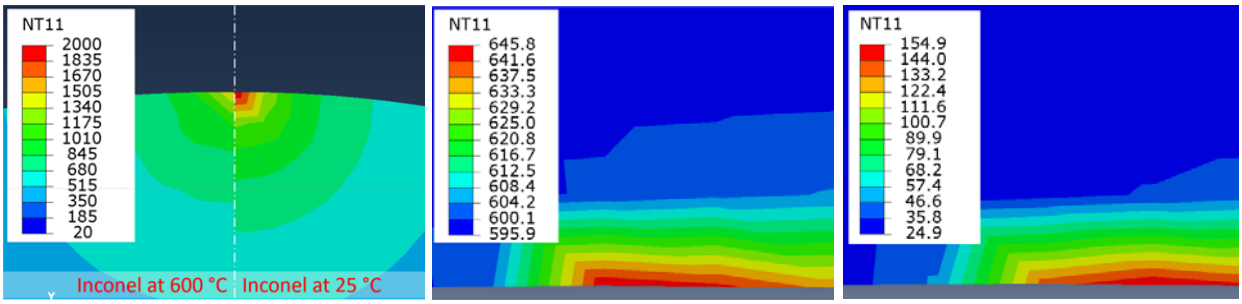

(a) (b) (c)

Fig. 9 FE generated contours of nodal temperature at the contact zone (5 m/s) (a) ceramic tip, (b) Inconel 718 in HT-test, and (c) Inconel 718 in RT-test.

3.3 Wear mechanism evolution of ceramics

In order to study the evolution of the contact zone, microscopic analysis was carried out. The wear surface morphology of the ceramic in HT-tests is shown in Fig. 10. The light grey areas are metallic transfer layers caused by adhesion of Inconel 718. Fig. 10b and c show what appears to be a brittle layer with cracks (marked as “tribochemical layer”). This tribochemical layer initially forms at 5 m/s in small quantities (Fig. 10b) and becomes larger and thicker (as will be shown in the cross-sectional analysis) at 7.5 m/s (Fig. 10c). Almost no tribochemical layer exists on the wear surface of ceramic at a velocity of 10 m/s (Fig. 10d). In addition, it appears as if parts of the tribochemical layer detach from the ceramic exposing a rough fracture surface (Fig. 10c).

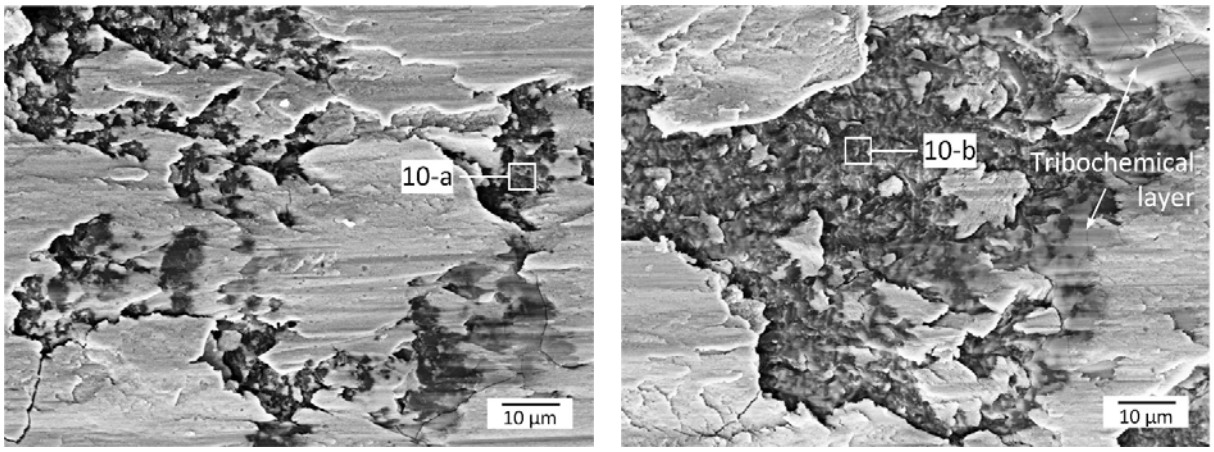

(a) (b)

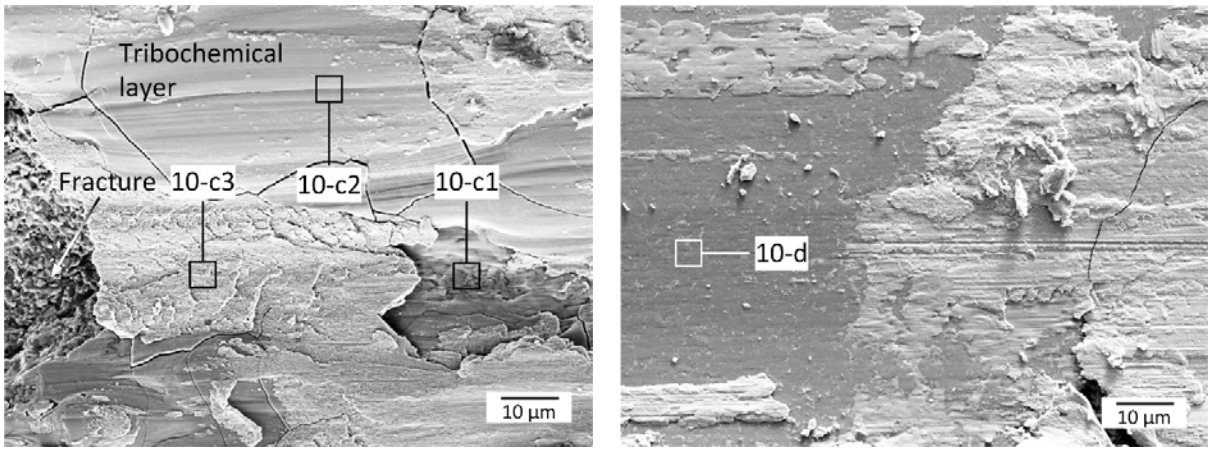

(c) (d)

Fig. 10 SEM images of wear surfaces of ceramic samples in HT-tests at sliding velocities of (a) 2.5 m/s, (b) 5.0 m/s, (c) 7.5 m/s, and (d) 10 m/s.

An EDX analysis was conducted to study the formation mechanism of the tribochemical layer, Fig. 11. The elemental analysis on zones 10-a, 10-b and 10-c1 (Fig. 10) indicate a decreasing content of Si and an increasing O content with increased velocity. Zone 10-c1 shows no traces of N. For zone 10-c3, the EDX analysis indicates elements consistent with the constituents of Inconel 718 with additional O content. As can be seen from 10-c2, the tribochemical layer is mainly composed of 60 at.% O and 28 at.% Cr, in addition to Nb, Al and Ti. The concentration of these elements in this layer is higher than that found in either the ceramic or Inconel 718. The zone 10-d is mainly silicon nitride.

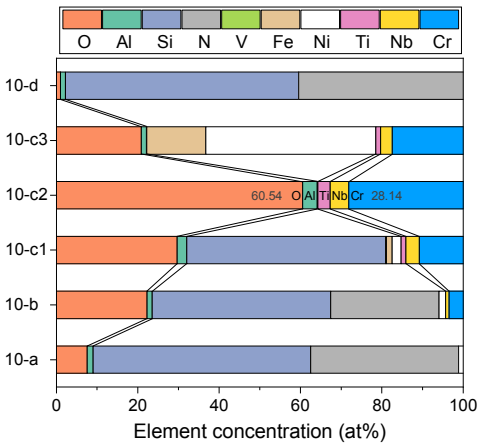

Fig. 11 EDX elemental analysis results on the ceramic surface (refer to Fig. 10).

A detailed microscope analysis of polished cross sections of ceramic sample for HT-tests was conducted in order to study the evolution of the contact zone, Fig. 12. At sliding velocity of 2.5 m/s, Inconel 718 adheres mechanically to the ceramic (Fig. 12a). At 5 m/s mechanically detached silicon nitride grains appear to be embedded into Inconel 718 (Fig. 12b). At 7.5 m/s and 10 m/s, the tribochemical layer appears between the ceramic and the metallic build-up, see Fig. 12c and d. The tribochemical layer

becomes thicker with increasing velocity (compare Fig. 12c and d). Similar to that shown in Fig. 10b and c, the tribochemical layer is prone to micro-cracking. A more detailed composition analysis at 12-c and 12-d was conducted. Zone 12-c shows high concentrations of O (39.1 at.%), Cr (19.9 at.%), Si (25.7 at.%), Al (4.8 at.%), and Ti (3.4 at.%), and low concentrations of Nb, Fe, and V. No trace of N was detected in this zone, which is similar to that at 10-c1 in Fig. 10. Zone 12-d shows higher concentrations of O (57.8 at.%), Cr (28.7 at.%), and Nb (5.2 at.%) but low Si concentration (0.3 at.%), the composition of which is similar to that at 10-c2 in Fig. 10.

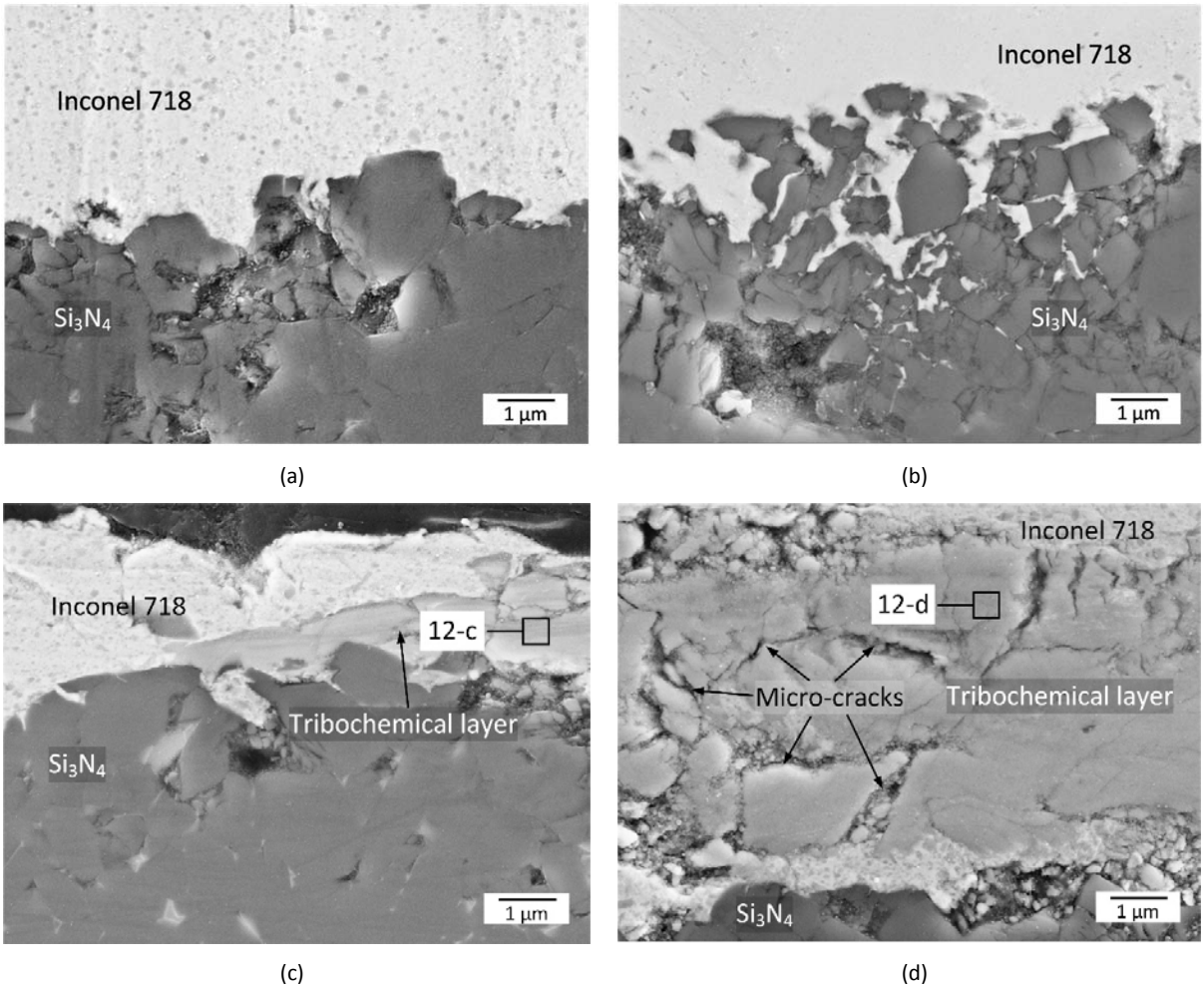

Fig. 12 SEM images of polished cross sections of ceramic samples in HT-tests at sliding velocities of (a) 2.5 m/s, (b) 5 m/s, (c) 7.5 m/s, and (d) 10 m/s.

For RT-tests, a cross-sectional analysis and the wear surface of the ceramic tested at 7.5 m/s and 10 m/s are shown in Fig. 13. No formation of tribochemical layer was observed upto 7.5 m/s. At 2.5 m/s and 5 m/s, the morphologies of cross sections were similar to that at 7.5 m/s as shown in Fig. 13a. It appears that the tribochemical layer has just started to form in small quantities at 10 m/s as shown in Fig. 13b and c.

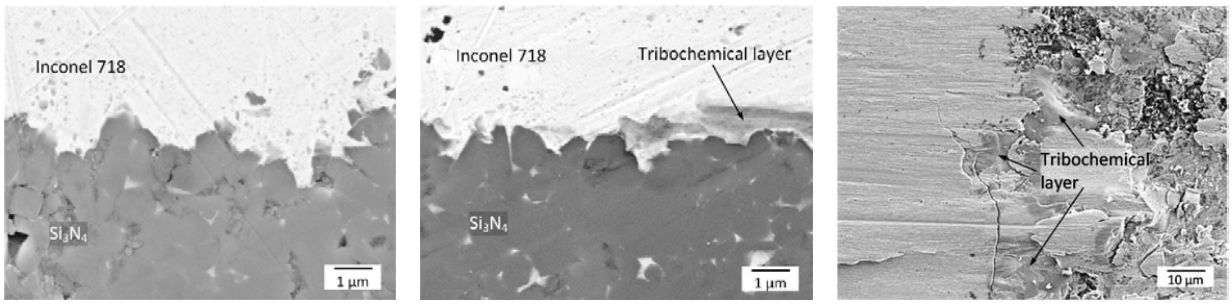

(a) (b) (c)

Fig. 13 SEM images of polished cross sections of ceramic samples in RT-tests at (a) 7.5 m/s and (b) 10 m/s, and (c) wear surface (10 m/s).

4 Discussion

The silicon nitride ceramic showed different tribological properties in RT-tests and HT-tests. Even though the COF in HT-tests is lower than that in RT-test, it should be pointed out that the wear rates of the ceramic were not always lower. Khader et al. [16] and Renz et al. [17] reported an increase in wear rates above a critical sliding velocity for silicon nitride based ceramics sliding against Inconel 718 at room temperature. It was attributed to tribochemical wear induced by extreme contact surface temperatures. Comparing the HT-tests (Fig. 10 and Fig. 12) and RT-tests (Fig. 13), it may be concluded that wear in the former is dominated by the formation of a tribochemical layer at lower sliding velocities. Such tribochemical layers have also been found in both dry sliding [16, 17] and in cutting processes [18, 26] for silicon nitride based ceramics. As seen in Fig. 11, the tribochemical layer mostly consists of oxygen and chromium. This O-Cr-rich tribochemical layer has a low melting point [27] and, thus, may lower the COF at high temperature due to its lubrication characteristics [28, 29]. Due to its brittleness and to the large difference in thermal expansion coefficient between silicon nitride ($\alpha_{SN\text{-}PU} = 1.9\times10^{-6}\ K^{-1}$-$3.0\times10^{-6}\ K^{-1}$ [24]) and the tribochemical layer (e.g., the thermal expansion coefficient of chromium oxide is $\alpha_{Cr2O3} = 9.8\times10^{-6}\ K^{-1}$ [30]), the layer becomes prone to microcracking as shown in Fig. 10 and Fig. 12. The microcrack density seems to increase with increasing sliding velocity leading to crack coalescence. As a consequence, the tribochemical layer becomes unstable and detaches from ceramic surface leaving a rough fracture surface as revealed in Fig. 10c. Moreover, the shear strength of the tribochemical layer is lower than that of Inconel 718 (for instance when considering the shear strength of chromium oxide [31, 25]). The fact that the 10 m/s tests did not show much tribochemical layer on the surface supports the hypothesis that the layer is easily sheared off under the influence of mechanical force.

In addition, the EDX confirmed the presence of elements, such as Al, Ti, and Nb, that most probably diffuses into the tribochemical layer at high temperature, refer to Fig. 11. Addhoum [26] and Çelik [32] reported similar diffusion layer formation with high Cr, Nb and Al concentration in high temperature

diffusion experiments between Inconel 718 and SiAlON ceramics. Chromium oxide can form a solid solution with aluminum oxide over the full range of compositions [33]; therefore, the oxidation of Cr promotes the diffusion of Al, both from silicon nitride and Inconel 718 into the tribochemical layer. Al, Ti, and Nb are key elements in strengthening phases, i.e., hardening precipitates γ'' (Ni_3Nb) and intermetallic precipitates γ' ($Ni_3(Ti,Al)$) in Inconel 718 [34]. Thus, the strength of Inconel 718 may be weakened due to the diffusion of Al, Ti, and Nb. Moreover, the maximum contact temperature of Inconel 718 in HT-tests reaches around 650 °C (Fig. 9b), which can be enough to cause strength reduction of Inconel 718 [10, 25] and promote diffusion. As shown in Fig. 7, the amount of metallic transfer layer in both RT-tests and HT-tests is almost similar. Therefore, the lower COF observed in HT-tests may be attributed to both the lubricating effect of the tribochemical layer and the strength degradation of the adhered metallic transfer layer on the surface of silicon nitride.

The COF is proportional to the frictional power, which explains the lower contact surface temperature of the ceramic in HT-tests compared to RT-tests. Moreover, low surface contact temperature is beneficial for the retention of the mechanical properties of the ceramic. Unlike that in the ceramic, the peak temperature computed for Inconel 718 in RT-tests is low and not enough to weaken the strength of the nickel-based alloy. So, it may be argued that laser heating gives rise to a temperature distribution more favorable in reducing wear in the ceramic pin.

Given the temperature distribution shown in Fig. 9, it may be concluded that high temperature on the Inconel 718 side (observed in the HT-tests) promotes element diffusion and oxidation, which plays a decisive role in the formation of the tribochemical layer. Even though the temperature of ceramic in HT-tests is lower, it is still high enough to cause oxidation of silicon nitride. Referring back to zones 10-c1, 10-c2 and 10-c3 shown in Fig. 10, it can be concluded that both silicon nitride and Inconel 718 oxidize during the HT-test, resulting in the formation of a tribochemical layer. On the other hand, no traces of Si were found in that tribochemical layer even though the content of Si is high in neighboring zones such as 10-c1. Similar results were also reported by [16, 18] and found in static interaction couple tests of Inconel 718 in contact with silicon-based ceramics by Mehan and McKee [35, 36]. It was argued that most of the Si atoms were dissolved by Inconel 718. The amount of Al is increased from 10-a, 10-b to 10-c1 zones, indicating that the Al_2O_3 that is contained in the grain boundary phase of silicon nitride plays an important role in the formation of the tribochemical layer.

A simplified schematic model of the wear behavior of the tested silicon nitride in HT-tests is proposed in Fig. 14. With increasing sliding velocity, the high contact temperature exacerbates the oxidation and diffusion wear. The SEM/EDX analysis shown in Fig. 10 and Fig. 11 reveal that the oxidation of silicon nitride to silicon oxide intensifies with increasing velocities. At 10 m/s, the tribochemical layer becomes

thick and moves away from ceramic surface, promoting tribochemical wear at the expense of mechanical wear.

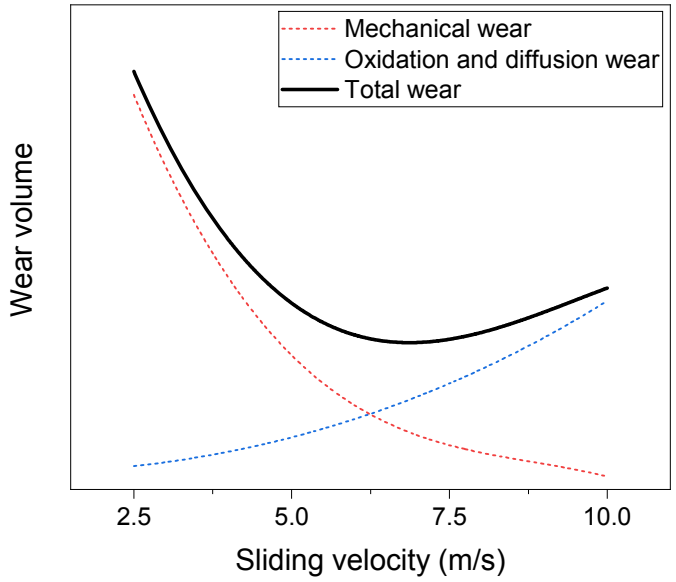

Fig. 14 Proposed wear mechanism evolution in silicon nitride in drying sliding against Inconel 718 (HT-tests).

5 Conclusions

The high temperature tribological behavior of a commercial silicon nitride ceramic was investigated under dry sliding contact against laser-heated (HT-tests) and unheated (RT-tests) Inconel 718. The analysis of wear was studied by means of pin-on-disk experiments and supported by finite element simulations. The following points can be concluded:

The COF in HT-tests were lower than those in RT-tests throughout the tested velocity regime. The wear rates of silicon nitride in HT-tests were lower than those in RT-tests up to 7.5 m/s. At 10 m/s, the ceramic wear rate in HT-tests was higher.

With laser heating to 600 °C, Inconel 718 reached a surface contact temperature of ca. 650 °C, which could cause a decrease in strength and promotes the diffusion rate of elements to form a lubricating tribochemical layer, resulting in a reduction of COF in HT-tests. The simulations indicated lower contact surface temperature in HT-tests, which can be attributed to the lower COF and consequently lower frictional power. Laser heating gave rise to a temperature distribution that is more likely to reduce wear rate of the ceramic.

With increasing sliding velocity, tribochemical wear becomes intensified, thus, increasing the wear of silicon nitride. Hence, laser-assisted heating of Inconel 718 may reduce wear rates in the ceramic up to a certain critical velocity (in this study 7.5 m/s), after which it promotes tribochemical wear at the expense

of mechanical wear. Thus, it is not recommended to use silicon nitride ceramics at velocities exceeding the critical velocity in high-temperature machining of Inconel 718.

Acknowledgements

This work has received funding from the Sino-German (CSC-DAAD) Postdoc Scholarship Program 2018 [57395819] supported by China Scholarship Council (CSC) and German Academic Exchange Service (DAAD) in addition to partial funding from the European Union's RFCS under grant agreement no. 7099920 "ReduWearGuid".

References

[1] D. Dudzinski, A. Devillez, A. Moufki, D. Larrouquère, V. Zerrouki and J. Vigneau, "A review of developments towards dry and high speed machining of Inconel 718 alloy," *International Journal of Machine Tools and Manufacture,* vol. 44, no. 4, pp. 439-456, 2004.

[2] B. Zhao, H. Liu, C. Huang, J. Wang, B. Wang and Y. Hou, "Cutting performance and crack self-healing mechanism of a novel ceramic cutting tool in dry and high-speed machining of Inconel 718," *The International Journal of Advanced Manufacturing Technology,* pp. 1-8, 2019.

[3] B. Zhao, H. Liu, C. Huang, J. Wang, M. Cheng and Q. Zhan, "Evolution mechanisms of high temperature mechanical properties and microstructures of Al2O3/SiCw/TiCn nanocomposite materials," *Journal of Alloys and Compounds,* vol. 737, pp. 46-52, 2018.

[4] V. Bushlya, J. Zhou, P. Avdovic and J. E. Ståhl, "Wear mechanisms of silicon carbide-whisker-reinforced alumina (Al2O3–SiCw) cutting tools when high-speed machining aged Alloy 718," *The International Journal of Advanced Manufacturing Technology,* vol. 68, no. 5-8, pp. 1083-1093, 2013.

[5] X. Tian, J. Zhao, J. Zhao, Z. Gong and Y. Dong, "Effect of cutting speed on cutting forces and wear mechanisms in high-speed face milling of Inconel 718 with Sialon ceramic tools," *The International Journal of Advanced Manufacturing Technology,* vol. 69, no. 9-12, pp. 2669-2678, 2013.

[6] G. Zheng, J. Zhao, Z. Gao and Q. Cao, "Cutting performance and wear mechanisms of Sialon–Si3N4 graded nano-composite ceramic cutting tools," *The International Journal of Advanced Manufacturing Technology,* vol. 58, no. 1-4, pp. 19-28, 2012.

[7] W. Akhtar, J. Sun, P. Sun, W. Chen and Z. Saleem, "Tool wear mechanisms in the machining of Nickel based super-alloys: A review," *Frontiers of Mechanical Engineering,* vol. 9, no. 2, pp. 106-119, 2014.

[8] R. P. Zeilmann, F. Fontanive and R. M. Soares, "Wear mechanisms during dry and wet turning of Inconel 718 with ceramic tools," *The International Journal of Advanced Manufacturing Technology,* vol. 92, no. 5-8, pp. 2705-2714, 2017.

[9] Y. Tian, B. Wu, M. Anderson and Y. Shin, "Laser-assisted milling of silicon nitride ceramics and inconel 718," *Journal of Manufacturing Science and Engineering,* vol. 130, no. 3, pp. 361-374, 2008.

[10] M. Anderson, R. Patwa and Y. C. Shin, "Laser-assisted machining of Inconel 718 with an economic analysis," *International Journal of Machine Tools & Manufacture,* vol. 46, no. 14, pp. 1879-1891, 2006.

[11] G. Germain, J. L. Lebrun, T. Braham-Bouchnak, D. Bellett and S. Auger, "Laser-assisted machining of Inconel 718 with carbide and ceramic inserts," *International Journal of Material Forming,* vol. 1, pp. 523-526, 2008.

[12] V. García-Navas, I. Arriola, O. Gonzalo and J. Leunda, "Mechanisms involved in the improvement of Inconel 718 machinability by laser assisted machining (LAM)," *International Journal of Machine Tools and Manufacture,* vol. 74, pp. 19-28, 2013.

[13] H. Attia, S. Tavakoli, R. Vargas and V. J. Thomson, "Laser-assisted high-speed finish turning of superalloy Inconel 718," *CIRP Annals-Manufacturing Technology,* vol. 59, no. 1, pp. 83-88, 2010.

[14] C. Huang, B. Zou, Y. Liu, S. Zhang, C. Huang and S. Li, "Study on friction characterization and wear-resistance properties of Si3N4 ceramic sliding against different high-temperature alloys," *Ceramics International,* vol. 42, no. 15, pp. 17210-17221, 2016.

[15] M. A. Shalaby and S. C. Veldhuis, "Wear and tribological performance of different ceramic tools in dry high speed machining of Ni-Co-Cr precipitation hardenable aerospace superalloy," *Tribology Transactions,* vol. 62, no. 1, pp. 62-77, 2019.

[16] I. Khader, A. Renz and A. Kailer, "A wear model for silicon nitride in dry sliding contact against a nickel-base alloy," *Wear,* Vols. 376-377, pp. 352-362, 2017.

[17] A. Renz, I. Khader and A. Kailer, "Tribochemical wear of cutting-tool ceramics in sliding contact against a nickel-base alloy," *Journal of the European Ceramic Society,* vol. 36, no. 3, pp. 705-717, 2016.

[18] A. Çelik, M. Sert-Alağa, S. Turan, A. Kara and F. Kara, "Wear behavior of solid SiAlON milling tools during high speed milling of Inconel 718," *Wear,* Vols. 378-379, pp. 58-67, 2017.

[19] K. Niihara, R. Morena and D. P. H. Hasselman, "Evaluation of KIc of brittle solids by the indentation method with low crack-to-indent ratios," *Journal of Materials Science Letters,* vol. 1, pp. 13-16, 1982.

[20] M. M. Yovanovich, "Recent developments in thermal contact, gap and joint conductance theories and experiment," in *Proceedings of the Eighth International Conference*, San Francisco, CA, 1986.

[21] N. M. Ravindra, S. Abedrabbo, W. Chen, F. M. Tong, A. K. Nanda and A. C. Speranza, "Temperature-dependent emissivity of silicon-related materials and structures," *IEEE Transactions on Semiconductor Manufacturing,* vol. 11, no. 1, pp. 30-39, 1998.

[22] "Table of Total Emissivity," OMEGA Engineering inc., 2003-2015. [Online].

[23] G. A. Greenea, C. C. Finfrock and T. F. Irvine Jr., "Total hemispherical emissivity of oxidized Inconel 718 in the temperature range 300–1000°C," *Experimental Thermal and Fluid Science,* vol. 22, no. 3-4, pp. 145-153, 2000.

[24] *EU RFCS-2015, Reduction of Wear on Guiding Components in Hot Strip Mill - ReduWearGuid, ID: 709920.*

[25] "INCONEL® Alloy 718," Special Metals Corporation, Sept. 2007. [Online]. Available: www.specialmetals.com.

[26] H. Addhoum and D. Broussaud, "Interaction of ceramic cutting tools with nickel-based alloys," *Materials 3cience and Engineering A,* vol. 109, pp. 379-387, 1989.

[27] J. Yuan, G. S. Fox-Rabinovich and S. C. Veldhuis, "Control of tribofilm formation in dry machining of hardened AISI D2 steel by tuning the cutting speed," *Wear,* Vols. 402-403, pp. 30-37, 2018.

[28] G. Bolelli, V. Cannillo, L. Lusvarghi and T. Manfredini, "Wear behaviour of thermally sprayed ceramic oxide coatings," *Wear,* vol. 261, no. 11-12, pp. 1298-1315, 2006.

[29] G. S. Fox-Rabinovich, A. Kovalev, M. H. Aguirre, K. Yamamoto, S. C. Veldhuis, I. S. Gershman, A. Rashkovskiy, J. L. Endrino, B. D. Beake, G. Dosbaeva, D. Wainstein, J. Yuan and J. Bunting, "Evolution of self-organization in nano-structured PVD coatings under extreme tribological conditions," *Applied Surface Science,* vol. 297, pp. 22-32, 2014.

[30] A. M. Dymshits, P. I. Dorogokupets, I. S. Sharygin, K. D. Litasov, A. Shatskiy, S. V. Rashchenko, E. Ohtani, A. Suzuki and Y. Higo, "Thermoelastic properties of chromium oxide Cr2O3 (eskolaite) at high pressures and temperatures," *Physics and Chemistry of Minerals,* vol. 43, no. 6, pp. 447-458, 2016.

[31] N. J. Mosey and E. A. Carter, "Shear strength of chromia across multiple length scales: An LDA + U study," *Acta Materialia,* vol. 57, no. 10, pp. 2933-2943, 2009.

[32] A. Çelik, "Dopant-dependent diffusion behavior of SiAlON ceramics against Inconel 718 superalloy," *Ceramics International,* vol. 44, no. 14, pp. 17440-17446, 2018.

[33] D. H. Riu, Y. M. Kong and H. E. Kim, "Effect of Cr2O3 addition on microstructural evolution and mechanical properties of Al2O3," *Journal of the European Ceramic Society,* vol. 20, no. 10, pp. 1475-1481, 2000.

[34] A. Thomas, M. El-Wahabi, J. M. Cabrera and J. M. Prado, "High temperature deformation of Inconel 718," *Journal of Materials Processing Technology,* vol. 177, no. 1-3, pp. 469-472, 2006.

[35] R. L. Mehan and D. W. Mckee, "Interaction of metals and alloys with silicon-based ceramics," *Journal of Materials Science,* vol. 11, no. 6, pp. 1009-1018, 1976.

[36] A. Renz, Untersuchung des Verschleißverhaltens von keramischen Schneidstoffen im trockenen Gleitreibungskontakt mit Nickelbasislegierungen, PhD Thesis, Stuttgart: Fraunhofer Verlag, 2015.